same Au wire by (i) allowing it to collide with the Nb surface or (ii) performing field emission with it such that there was a significant change in the microscopic configuration of its outermost atoms. The results of these experiments show that the Au tips contribute little to the features in the spectra measured over the narrow range of energies near the Fermi level E_F, where we are interested in the DOS. Furthermore, our results were insensitive to the value of initial junction impedance (which determines the tip height) over 3.5 decades (10^8 to 5×10^5 ohms), except for a constant scaling factor.
8. A. Roy, D. S. Buchanan, D. J. Holmgren, D. M. Ginsberg, *Phys. Rev. B* **31**, 3003 (1985).
9. P. D. Scholten and W. G. Moulton, *ibid.* **15**, 1318 (1977).
10. P. Schlottmann, *ibid.* **13**, 1 (1976).
11. P. G. de Gennes, *Superconductivity in Metals and Alloys* (Addison-Wesley, Reading, MA, 1989).
12. Similar approaches have been used to describe STM measurements near a vortex [(*6*); J. D. Shore *et al*., *Phys. Rev. Lett.* **62**, 3089 (1989); F. Gygi and M. Schluter, *Phys. Rev. B* **41**, 822 (1990)]. For more recent calculations near a vortex, see N. Hayashi, M. Ichioka, K. Machida, *Phys. Rev. Lett.* **77**, 4074 (1996).
13. We have not made a more detailed comparison of the radial dependence between the measurement and the model calculation. Such a comparison would require us to taken into account the details of the adatom geometry, that is, the fact that at small lateral tip displacements ($r < 4$ Å), most of the tunneling current is channeled through the impurity site [for example, see N. D. Lang, *Phys. Rev. Lett.* **56**, 1164 (1986)].
14. Our model predicts a local electron-hole asymmetry that oscillates and decays as a function of distance from the impurity. The $l = 0$ amplitude remains constant, but its contribution decays as a function of r. Gaussian averaging of the model calculation over typical distances averaged by STM causes a nonoscillatory but decaying asymmetry in the region near the impurity.
15. A. Sakurai, *Prog. Theor. Phys.* **44**, 1472 (1970).
16. Varying the parameters of the calculation, we find that for $a = 2.5$ Å, we can fit the data using U ranging from 0 to 0.15 E_F, while allowing J to vary by 5%. The bound excitation energy, that is, the peak location in the data, is a very sensitive function of J.
17. M. E. Flatte and J. M. Byers, *Phys. Rev. Lett.*, in press.
18. M. I. Salkola, A. V. Balatsky, J. R. Schrieffer, *Phys. Rev. B*, in press.
19. We thank the authors of (*17*) and (*18*) for their interest in our experiment and thank D.-H Lee, D. J. Scalapino, and M. Tinkham for fruitful discussions.

21 November 1996; accepted 3 February 1997

Novel Colloidal Interactions in Anisotropic Fluids

Philippe Poulin, Holger Stark,* T. C. Lubensky, D. A. Weitz

Small water droplets dispersed in a nematic liquid crystal exhibit a novel class of colloidal interactions, arising from the orientational elastic energy of the anisotropic host fluid. These interactions include a short-range repulsion and a long-range dipolar attraction, and they lead to the formation of anisotropic chainlike structures by the colloidal particles. The repulsive interaction can lead to novel mechanisms for colloid stabilization.

Dispersions of small particles in a host fluid are a widespread and important state of matter (*1*); colloidal suspensions are dispersions of solid particles, whereas emulsions are dispersions of liquid droplets coated with a surfactant. They are of considerable technological importance, with applications in everything from paints and coatings to foods and drugs. These are metastable rather than equilibrium systems. Attractive interactions among the particles, which arise, for example, from dispersion forces, can separate the dispersed phase from the host fluid. These forces must be counterbalanced by Coulombic, steric, or other repulsive interactions. The delicate balance between attractive and repulsive colloidal interaction determines the stability and hence usefulness of dispersions.

We report on a novel class of colloidal interactions that arise when the host fluid is anisotropic and provide a comprehensive theoretical framework to understand them. These interactions have both repulsive and attractive components. We use general theoretical arguments and a variational procedure based on analogies with electrostatics to show how these interactions arise from the orientational elasticity of the host fluid and from topological defects therein induced by the dispersed particles. The nature of these interactions depends on boundary conditions and on the anisotropy direction of the host fluid at particle and other interfaces. Modifications in these boundary conditions can easily be produced through changes in the composition of the surfactant or host fluid, making possible a fine degree of control of colloidal interactions.

We dispersed water droplets 1 to 5 μm in diameter in a nematic liquid crystal (LC) host, pentylcyanobiphenyl (5CB), with a small amount of surfactant added to help stabilize the interface. We also used multiple emulsions, in which the nematic LC host was itself a much larger drop (~50 μm in diameter) in a continuous water phase; this isolated a controlled number of colloidal droplets in the nematic host and allowed us to readily observe their structure. The multiple emulsions were formed with sodium dodecyl sulfate, a surfactant that is normally ineffective at stabilizing water droplets in oil. Nevertheless, the colloidal water droplets remained stable for several weeks, which suggested that the origin of this stability is the surrounding LC—a hypothesis that was confirmed by the observation that droplets became unstable and coalesced in <1 hour after the LC was heated to the isotropic phase.

We studied these nematic emulsions by observing them between crossed polarizers in a microscope. Between crossed polarizers, an isotropic fluid will appear black, whereas nematic regions will be colored. Thus, the large nematic drops in a multiple emulsion are predominately red in Fig. 1A, whereas the continuous water phase surrounding them is black. Dispersed within virtually all of the nematic drops are smaller colloidal water droplets, which also appear dark in the photo; the number of water droplets tends to increase with the size of the nematic drops. In all cases, the water droplets are constrained at or very near the center of the nematic drops. Moreover, their Brownian motion has completely ceased, an observation that is confirmed by warming the sample to change the nematic into an isotropic fluid, whereupon the Brownian motion of the colloidal droplets is clearly visible in the microscope.

Perhaps the most striking observation in Fig. 1A is the behavior of the colloidal droplets when two or more cohabit the same nematic drop: The colloidal droplets invariably form linear chains. This behavior is driven by the nematic LC—the chains break, and the colloidal droplets disperse immediately upon warming the sample to the isotropic phase. However, although the anisotropic LC must induce an attractive interaction to cause the chaining, it also induces a shorter range repulsive interaction. A section of a chain of droplets under higher magnification (Fig. 1B) shows that the droplets are prevented from approaching too closely, with the separation between droplets being a significant fraction of their diameter.

A clue to the origin of these new interactions comes from close examination of the patterns produced by the nematic host. Nematic drops containing only a single emulsion droplet invariably exhibit a distinctive four-armed star of alternating bright and dark regions that extend throughout the whole nematic drop (Fig. 1C). This pattern is produced by the rotation of the nematic anisotropy axis through a full 360° about the central water droplet and is characteristic of a topological defect called a hedgehog (*2*). When there is more than one water droplet, there is additional orientational texture between every pair of

Department of Physics and Astronomy, University of Pennsylvania, Philadelphia, PA 19104, USA.

*Present address: Institut für Theoretische und Angewandte Physik, Universität Stuttgart, Pfaffenwaldring 57, D-70550, Stuttgart, Germany.

droplets. This structure is a distorted four-arm star, which we identify as a hedgehog defect created in the nematic host. The distance between droplets and this host-fluid defect increases with increasing droplet radius. Moreover, there is always one less host defect than there are water droplets.

Colloidal water droplets can also be dispersed in a nematic host confined between parallel plates treated to force molecular alignment parallel to their surfaces. The droplets still form chains, but over time these chains continue to grow into larger and more complicated structures. Exactly one host defect is associated with each water droplet, so each chain has as many extra defects as water droplets rather than one less. We conclude that water droplets create defects in the host fluid that prevent close contact between water droplets and that give rise to a long-range anisotropic attractive interaction between droplets.

To explain these observations, we consider the properties of the unit vector field $\mathbf{n}(\mathbf{r})$, called the Frank director, that specifies the direction of local alignment of anisotropic LC molecules (*3*) at the point $\mathbf{r} = (x, y, z)$. Nematics are invariant under the inversion operation $\mathbf{n}(\mathbf{r}) \rightarrow -\mathbf{n}(\mathbf{r})$. The energy of long-wavelength, spatially nonuniform distortions of $\mathbf{n}$ is determined by the Frank free energy (F), which in the one-elastic constant approximation is

$$F = \frac{1}{2} \sum_{i,j} \int d^3r \nabla_i n_j \nabla_i n_j \qquad (1)$$

where the integral is over the volume of the nematic LC; $i,j = x, y, z$; n_i is the i^{th} component of the director, and $\nabla_i = \partial/\partial x_i$. The elastic constant K is of order 10^{-6} dynes in typical nematics. We must also consider topological defects in nematics, an important example of which is a hedgehog: a point defect in which the director sweeps out all directions on the unit sphere as all points on any surface enclosing the defect core are visited. Hedgehogs are characterized by an integer topological charge specifying the number of times the unit sphere is wrapped. These hedgehogs can have different director configurations. The simplest is the radial hedgehog, in which the director $\mathbf{n}(\mathbf{r}) = (x, y, z)/r$ points radially outward like the electric field of a point charge. Another common configuration is the hyperbolic hedgehog with $\mathbf{n} = (-x, -y, z)/r$ (Fig. 2A) obtained from the radial hedgehog by rotating all vectors by 180° about the z axis. These hedgehogs can be characterized by a topological charge of 1. However, the nematic inversion symmetry renders positive and negative charges indistinguishable, so that two unit-charge hedgehog defects can be combined to give configurations with a total topological charge of either 2 or 0. In addition to hedgehogs, topological line defects called disclinations can also exist in nematics. Although there have been conjectures (*4*, *5*) that a colloidal particle in a nematic will nucleate a disclination ring centered at its equator, we have found no experimental evidence for this for particles of the size we investigate.

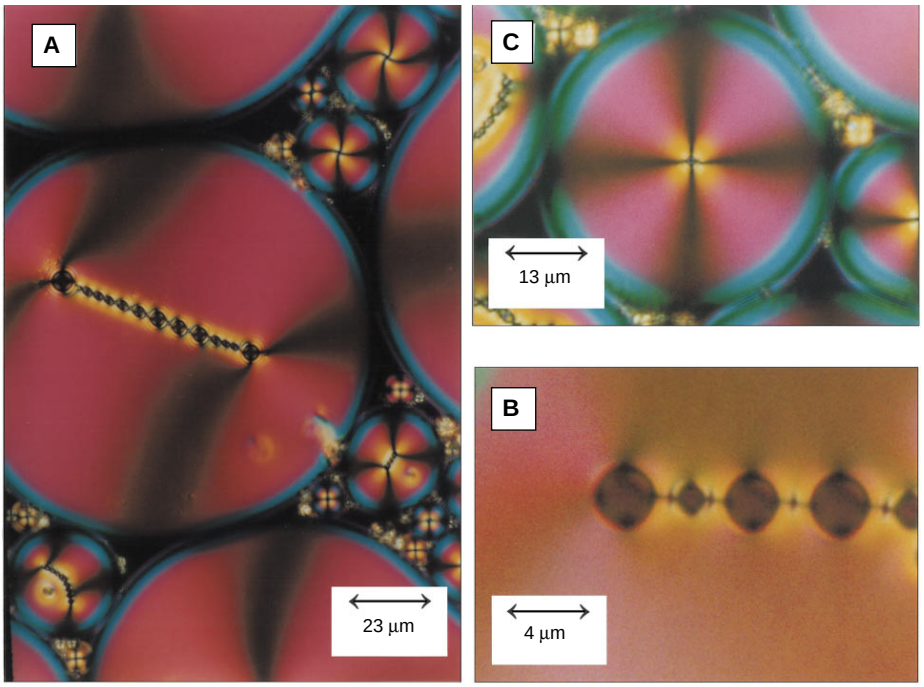

Fig. 1. (**A**) Microscope image of a nematic multiple emulsion taken under crossed polarizers. (**B**) A chain of water droplets under high magnification. (**C**) A nematic drop containing a single water droplet.

Our observations can be qualitatively explained by considering the total topological charge Q in a nematic, which is determined by boundary conditions on $\mathbf{n}$. Parallel boundary conditions at infinity force Q to be 0, whereas normal or homeotropic boundary conditions on a closed surface with the topology of a sphere force Q to be 1. Normal boundary conditions at the water droplet surfaces force the creation of a radial hedgehog at each droplet. Thus, for homeotropic boundary conditions, a single hedgehog in a closed nematic drop with a single water droplet can satisfy both the boundary condition at the water droplet and the requirement $Q = 1$. Our observation of a single four-armed texture in single-droplet nematic drops is in accord with this. Each water droplet beyond the first added to the interior of a nematic drop must create orientational structure out of the nematic itself to satisfy the global constraint $Q = 1$. Similar considerations apply to each water droplet, including the first, added to a nematic cell with $Q = 0$. The simplest (though not the only) way to satisfy this constraint is for each extra water droplet to create a hyperbolic hedgehog in the nematic host (*6*). The radial droplet hedgehog and the companion host-liquid

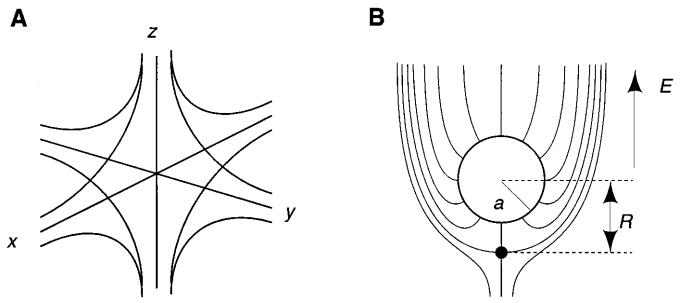

Fig. 2. (**A**) Director configuration for a hyperbolic defect. The director is tangent to the lines shown. (**B**) A droplet-defect dipole. The director configuration around the spherical droplet is that of a radial hedgehog. The point defect is a hyperbolic hedgehog. Rotation of this figure about the vertical axis produces the three-dimensional director configuration, which is uniform and parallel to the vertical axis from the dipole. In the electrostatic analog, the droplet becomes a conducting sphere with charge Q in an external electric field E, which produces the field lines determining the orientation of the director.

hyperbolic hedgehog combine to create a parallel director pattern at infinity (Fig. 2B). All of our experimental observations—including the observation of one host defect per water droplet in the nematic between parallel plates and $N - 1$ host defects for N water droplets in a nematic drop—are consistent with this simple scenario.

We can use Eq. 1 to determine the energy E_D of the droplet-defect dipole as a function of the separation R between the defect and the droplet center and thereby obtain the equilibrium separation R_0. Simple dimensional analysis and more detailed calculations (7) show that this energy grows linearly with separation R for R much greater than the droplet radius a. Energy increases as R approaches a (Fig. 2B): The director has to change directions from vertical to horizontal in a distance of order $R - a$ leading to $\nabla\mathbf{n} \sim 1/(R - a)$ in Eq. 1. Beyond a distance of order R from the sphere, the director is approximately uniform. Thus, $E_D \sim [K/(R - a)^2][AR^3 - (4\pi/3)a^3]$, where A is a number of order unity. This energy is linear in R at large R, diverges as R approaches a, and has a minimum at some $R_0 \sim a$. To obtain a more reliable estimate, we constructed a variational ansatz for the unit vector field, $\mathbf{n}(\mathbf{r})$, that is parallel to the z axis at infinity, that is perpendicular to the surface of the droplet, and that has a companion hyperbolic defect somewhere. A vector field satisfying these conditions can be obtained from the electrostatic problem of a conducting sphere of positive charge Q in a uniform electric field $\mathbf{E}_0 = E_0\mathbf{e}_z$ parallel to the z axis as shown in Fig. 2. In reduced units with $\tilde{\mathbf{r}} = \mathbf{r}/a = (\tilde{x}, \tilde{y}, \tilde{z})$, the solution to this problem for a sphere at the origin yields an electric field $\mathbf{E}(\mathbf{r})/E_0 = \mathbf{e}_z + \lambda^2\tilde{\mathbf{r}}/\tilde{r}^3 - \tilde{r}^{-5}(\tilde{r}^2\mathbf{e}_z - 3\tilde{z}\tilde{\mathbf{r}})$, where $\lambda^2 = Q/E_0a^2$. This field arises from the external field, the charge on the sphere, and an induced dipole at the center of the sphere. There is no negative electric charge in this problem, but there is a point where the electric field goes to zero (provided λ^2 is sufficiently large). The electric field configuration in the vicinity of this point is identical to that of a unit vector field in the vicinity of a hyperbolic hedgehog defect. Thus, a variational ansatz for the director that satisfies all of our conditions is $\mathbf{n}(\mathbf{r}) = \mathbf{E}(\mathbf{r})/|\mathbf{E}(\mathbf{r})|$. At distances $r \gg a$

$$\mathbf{n}(\mathbf{r}) \approx \left(\lambda^2 a^2 \frac{x}{r^3}, \lambda^2 a^2 \frac{y}{r^3}, 1\right) \qquad (2)$$

and n_x and n_y are solutions to Laplace's equation as they must be to minimize F. The zero of the electric field and thus the distance $R = |\tilde{z}|a$ to the hyperbolic defect is determined by the solution to $|\tilde{z}|^3 - \lambda^2|\tilde{z}| + 2 = 0$. We can therefore use our ansatz for $\mathbf{n}(\mathbf{r})$ in Eq. 1 to obtain an estimate of E_D as a function of reduced separation $\tilde{R} = |\tilde{z}|$ (Fig. 3A). This energy is linear in $\tilde{R}$ at large $\tilde{R}$ and has a minimum of $13.00\pi Ka$ at $R_0 = 1.17a$. The curvature is $33\pi Ka$ indicating that thermal fluctuations in the reduced separation between droplet and hyperbolic hedgehog is negligible: $(\delta\tilde{R}_0)^2 \approx kT/33\pi Ka \approx 10^{-5}$, where $\delta\tilde{R} = \tilde{R} - \tilde{R}_0$, k is the Boltzmann constant, and T is the temperature. A well-defined distance, R_0, separates a colloidal water droplet from its companion defect, and this distance scales with the droplet radius. A host defect between two water droplets, therefore, prevents the water droplets from approaching each other too closely; it provides a repulsive barrier between two water droplets.

To treat long-range attractive interactions between droplets that lead to chaining, we seek a phenomenological free energy (5) describing how the water droplet distorts the director field at distances that are large compared to R_0. This energy must produce the large-R director field predicted by Eq. 2. The droplet-defect pair has vector symmetry, and we assign it a dipole moment $\mathbf{p} = (\lambda a)^2\mathbf{e} \equiv p\mathbf{e}$, where $\mathbf{e}$ is the unit vector from the companion defect to the droplet center. From this we can construct a dipole-moment density for a collection of defects at positions $\mathbf{r}_\alpha$ with respective dipole moments $\mathbf{p}_\alpha$: $\mathbf{P}(\mathbf{r}) = \sum_\alpha \mathbf{p}_\alpha\delta(\mathbf{r} - \mathbf{r}_\alpha)$. We now seek a free energy that, upon minimization, will lead to Eq. 2 for a single defect located at the origin with $\mathbf{p}$ pointing in the minus z direction:

$$F = K\int d^3r\left[\frac{1}{2}\sum(\nabla_i n_j)(\nabla_i n_j) - 4\pi\mathbf{P}(\mathbf{r})\cdot\mathbf{n}(\nabla\cdot\mathbf{n})\right] - \frac{1}{2}A\sum_\alpha[\mathbf{p}_\alpha\cdot\mathbf{n}(\mathbf{r}_\alpha)]^2 \qquad (3)$$

The second term in this energy is a flexoelectric term (8), and the last term (with an as-yet-unmeasured coefficient A) results from the energetic preference for the dipoles to align either parallel or antiparallel to the director. Minimization of Eq. 3 over $\mathbf{n}$ for a single defect at the origin [$\mathbf{P} = p\mathbf{e}_z\delta(\mathbf{r})$] for small deviations from linear equilibrium leads to $n_i(\mathbf{r}) = pr_i/r^3$ for $i = x,y$. This reproduces Eq. 2 for $p = \lambda^2a^2$.

The tendency to form chains can be explained by the effective dipole-dipole interaction predicted by Eq. 3. By calculating the director field at $\mathbf{r}'$ produced by a dipole moment density at $\mathbf{r}$, we can calculate the effective dipole-dipole potential:

$$U_{\alpha\beta} = 4\pi K p_\alpha^z p_\beta^z \frac{1 - 3\cos^2\theta}{R^3} \qquad (4)$$

where θ is the angle between $\mathbf{R} = \mathbf{r}_\alpha - \mathbf{r}_\beta$ and the z axis. p_α^z is the component of the dipole moment of defect α along the z axis; it can be either positive or negative. This energy is clearly minimized when p_α^z and p_β^z have the same sign (that is, $\mathbf{p}_\alpha$ and $\mathbf{p}_\beta$ point in the same direction) and their separation vector is parallel to the z axis. This form accounts for the attractive interaction and leads to the formation of chains as seen in experiments. It is similar to configurations seen in other dipole systems such as electrorheological fluids and in magnetic emulsions (9).

The predicted scale for both the dipole-dipole attractive and defect-mediated repulsive interactions should be set by the droplets' diameter; as a consequence, the droplet separation within the chains should scale with a. To test this hypothesis, we measured the separations between the surfaces of neighboring droplets as their radius increased, and the results are plotted in Fig. 3B. A linear increase was observed. Moreover, the fit to the data (solid line) gives $S \approx 0.6a$. This value is in good accord with the expectation that the distance between droplets be somewhat greater than twice the separation $2(R_0 - a)$ between a droplet and its companion defect.

The model free energy of Eq. 3 also accounts for several other experimental observations. It incorporates a preference for $\mathbf{p}$ to align along $\mathbf{n}$. This was verified by observing single droplets between parallel glass plates treated to force tangential alignment of the director at their surface; $\mathbf{p}$ is invariably aligned with $\mathbf{n}$. In addition, Eq. 3 also predicts that the defects will seek regions with maximum director splay ($\nabla\cdot\mathbf{n}$) and that $\mathbf{p}$ will prefer to orient antiparallel

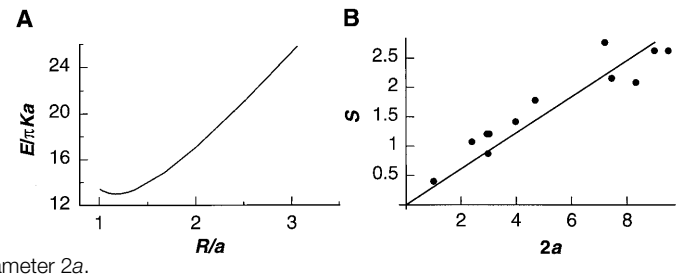

Fig. 3. (**A**) Plot of reduced energy $E/\pi Ka$ of a droplet-negative hedgehog as a function of reduced separation R/a. Note the linear dependence at large $\tilde{T}$ and the minimum at $R_0 \approx 1.17a$. (**B**) Plot of the distance d between droplet surfaces as a function of their diameter $2a$.

to **n** when $\nabla \cdot \mathbf{n}$ is positive. A nematic drop with $Q = 1$ has nonvanishing positive splay everywhere. This splay acts as an external field that establishes minimum energy positions for droplet dipoles and thereby arrests Brownian motion. The minimum energy position of a single droplet is at the center of a nematic drop. A second droplet moves to maximum splay at the center with **p** pointing toward the center along negative **n** in accord with observations. Subsequent droplets form chains. In contrast, in the parallel geometry there is no splay localizing particles; as a result, the particles and chains undergo Brownian motion, which leads to interchain coagulation.

Finally, one of the most important features of these novel colloidal interactions is their dependence on the anchoring of the nematic at the interface. For example, the behavior of the colloidal droplets in the multiple emulsions is completely altered if the nematic is forced to align parallel to the surface of the large droplets rather than perpendicular. In the passage from homeotropic to tangential alignment, the topological charge interior to a nematic drop is changed from 1 to 0, and point defects called boojums (*2*) develop on its surface. Splay is a maximum in the vicinity of these boojums, and thus we would expect the colloidal droplets to congregate at these defects. We can achieve tangential boundary conditions at the surface of the nematic drops, but not at the surfaces of interior colloidal water droplets, by adding a small amount of glycerol to the continuous water phase. As expected, the colloidal droplets do indeed migrate to the boojums. Similarly, in our theory, both the chaining and the defect-mediated repulsion are a consequence of the dipolar defect configuration produced by a droplet with homeotropic boundary conditions. Droplets with tangential boundary conditions create neither a radial nor a companion hyperbolic hedgehog and should, therefore, exhibit completely different structures. To test this, we added polyvinyl alcohol to the water droplets to change boundary conditions from homeotropic to tangential. The tendency to form chains was greatly reduced; moreover, the droplets were no longer separated by large distances when they approached one another, reflecting the absence of the hedgehog defects.

The new class of colloidal interactions discussed in this paper is not restricted to thermotropic nematic LC but should be present whenever the host fluid is anisotropic. Interesting effects can be expected as the delicate balance among the magnitude of the elastic constant, the particle size, and the anchoring energies is adjusted. For example, this class of interactions should also be present for solutions of anisotropic micelles (*10*), rigid-rod polymers, and even biological systems such as actin or viruses. Moreover, the ability to controllably obtain both attractive and repulsive interactions offers an opportunity to develop novel routes to colloid stabilization and structure, as well as to create new materials with potentially useful applications. The theoretical picture presented here provides the framework for understanding all of these phenomena.

REFERENCES AND NOTES

1. W. B. Russel, D. A. Saville, W. R. Schowalter, *Colloidal Dispersions* (Cambridge Univ. Press, Cambridge, 1989).
2. M. V. Kurik and O. D. Lavrentovich, *Usp. Fiz. Nauk*, **154**, 381 (1988) [*Sov. Phys. Usp.* **31**, 196 (1988)]; N. D. Mermin, *Rev. Mod. Phys.* **51**, 591 (1979).
3. P. G. de Gennes and J. Prost, *The Physics of Liquid Crystals* (Clarendon, Oxford, ed. 2, 1993); S. Chandrasekhar, *Liquid Crystals* (Cambridge Univ. Press, Cambridge, 1992).
4. E. M. Terentjev, *Phys. Rev. E* **51**, 1330 (1995); O. V. Kuksenpk, R. W. Ruhwandl, S. V. Shiyanovskii, E. M. Terentjev, *ibid.* **54**, 5198 (1996).
5. S. Ramaswamy, R. Nityananda, V. A. Garhunathan, J. Prost, *Mol. Cryst. Liq. Cryst.* **288**, 175 (1996).
6. R. B. Meyer, *ibid.* **16**, 355 (1972).
7. S. Ostlund, *Phys. Rev. B* **24**, 485 (1981).
8. R. B. Meyer, *Phys. Rev. Lett.* **22**, 918 (1969).
9. A. P. Gast and C. F. Zukoski, *Adv. Colloid Interface Sci.* **30**, 153 (1989).
10. P. Poulin, V. A. Raghunathan, P. Richetti, D. Roux, *J. Phys. II France* **4**, 1557 (1994).

11. We are grateful to A. Yodh for helpful discussions and a careful reading of the manuscript and to F. Macera for help with the figures. Supported primarily by the Materials Research Science and Engineering Center Program of NSF under award number DMR96-32598.

30 September 1996; accepted 7 February 1997

Direct Radiometric Observations of the Water Vapor Greenhouse Effect Over the Equatorial Pacific Ocean

Francisco P. J. Valero,* William D. Collins, Peter Pilewskie, Anthony Bucholtz, Piotr J. Flatau

Airborne radiometric measurements were used to determine tropospheric profiles of the clear sky greenhouse effect. At sea surface temperatures (SSTs) larger than 300 kelvin, the clear sky water vapor greenhouse effect was found to increase with SST at a rate of 13 to 15 watts per square meter per kelvin. Satellite measurements of infrared radiances and SSTs indicate that almost 52 percent of the tropical oceans between 20°N and 20°S are affected during all seasons. Current general circulation models suggest that the increase in the clear sky water vapor greenhouse effect with SST may have climatic effects on a planetary scale.

Recent studies (*1*) have demonstrated that atmospheric general circulation models, when forced only with measured SSTs (in particular, tropical Pacific SSTs), can reproduce the changes in global tropospheric temperatures that have been observed during the last several decades (*2, 3*). Earlier results (*4–6*) also pointed to the existence of a relation between variations in the tropical Pacific SSTs and global tropospheric temperatures. In this context, the clear sky water vapor greenhouse effect is key to the understanding of climate change, including global warming (*7*). The greenhouse effect can be defined as (*8–10*)

$$G_a = \sigma(\mathrm{SST})^4 - F^+ \qquad (1)$$

According to the Stefan Boltzmann law, $\sigma(\mathrm{SST})^4$ is the infrared black body emission by the surface at temperature SST, $\sigma = 5.67 \times 10^{-8}$ W m^{-2} K^{-4} is the Stefan Boltzmann constant, and F^+ is the outgoing infrared radiation flux at the top of the atmosphere.

Satellite studies (*8–10*) have found that for clear skies and SSTs above 298 K, the spatial variation of G_a with SST, $dG_a/d(\mathrm{SST})$, exceeds the rate of increase of sea surface emission, $d\sigma(\mathrm{SST})^4/d(\mathrm{SST}) = 4\sigma(\mathrm{SST})^3$. For a tropical SST of 300 K, $4\sigma(\mathrm{SST})^3 \approx 6.1$ W m^{-2} K^{-1}. This effect, termed the "super greenhouse effect" (*11*), occurs in both hemispheres during all seasons. It is also observed for interannual variations of G_a with SST during the El Niño in the tropical Pacific (*12*). Observations in the tropical Atlantic ocean (*11*) show that the clear sky downwelling infrared flux incident on the surface (F_a^-) also increases faster than the surface emission with increasing SST. The net result is fur-

F. P. J. Valero, W. D. Collins, A. Bucholtz, P. J. Flatau, Atmospheric Research Laboratory, Center for Atmospheric Sciences, Scripps Institution of Oceanography, University of California, San Diego, 9500 Gilman Drive, La Jolla, CA 92093–0242, USA.
P. Pilewskie, NASA, Ames Research Center, Moffett Field, CA 94035, USA.
*To whom correspondence should be addressed.